Ultrasonics 53 (2013) 432–438

Contents lists available at SciVerse ScienceDirect

Ultrasonics

journal homepage: www.elsevier.com/locate/ultras

Application of the split-step Padé approach to nonlinear field predictions

Tomoo Kamakura [a,*], Hideyuki Nomura [a], Gregory T. Clement [b]

[a] Graduate School of Informatics and Engineering, The University of Electro-Communications, 1-5-1 Chofugaoka, Chofu-shi, Tokyo 182-8585, Japan
[b] Brigham and Women's Hospital, Harvard Medical School, 221 Longwood Ave., Boston, MA 02115, USA

ARTICLE INFO

Article history:
Received 21 April 2012
Received in revised form 4 August 2012
Accepted 4 August 2012
Available online 3 October 2012

Keywords:
Nonlinear acoustics
Split-step Padé approach
Parametric sound

ABSTRACT

We herein propose a new theoretical approach for analyzing the nonlinear propagation of directive sound beams emitted from a planar piston source with a circular aperture. The proposed approach relies on the split-step Padé approximation, which is an efficient method for obtaining wide-angle one-way wave equations, especially in underwater acoustics. Despite including only two Padé terms in the expansion, the theory was applicable to a beam angle of up to ±40° relative to the main propagation direction, the angle of which is approximately twice that of the Khokhlov–Zabolotskaya–Kuznetsov equation, which is based on parabolic approximation. In order to demonstrate the effectiveness of the newly proposed theoretical approach, we performed an experiment using an airborne ultrasonic emitter with a circular aperture of 7.5 cm in radius. We drove the emitter powerfully at a 36-kHz and 40-kHz bi-frequency signal and measured the beam patterns of the primary and secondary waves, such as parametric sounds within wide propagation angles. Excellent agreement between measured data and the corresponding numerical simulations supports the validity of the proposed model equations and the computational methods for their numerical solutions.

1. Introduction

The Khokhlov–Zabolotskaya–Kuznetsov (KZK) equation is widely used for theoretical prediction of the nonlinear field of a directive sound beam, especially when quantitative evaluations in harmonic and/or parametric sound generations are needed [1,2]. This model equation is derived from a full nonlinear wave equation known as the Westervelt equation under the conditions of one-way propagation and parabolic approximation. Unfortunately, the latter condition imposes two spatial limitations on its applicability. One limitation is that the field must be relatively far from a sound source, and the other limitation is that the paraxial region is a cone of up to approximately 20° with respect to the beam axis [2,3]. Hence, the KZK equation becomes inaccurate for theoretically describing the propagation of sound beams that are wider than 20°.

Several prospective approaches and techniques that do not require parabolic approximation have hitherto been proposed in order to overcome such applicability limitations. For example, Christopher and Parker used the convolution theorem and the discrete Hankel transform of a point spread function to describe a full diffractive wave with arbitrary absorption [4]. Tavakkoli et al. introduced the Rayleigh integral formula for solving the diffraction equation in the time domain [5], whereas Zemp et al. simulated diffraction fields using the angular spectrum method from the viewpoint of computational efficiency [6]. Huijssen et al. obtained the axial and lateral beam profiles of harmonic components by applying the FDTD scheme to the Westervelt model equation [7]. Furthermore, Huijssen and Verweij proposed a promising method that is based on the Neumann iterative solution of the Westervelt equation, where the nonlinear term is treated as a nonlinear contrast source [8]. Interestingly, their method is free of any assumed wavefield directionality. Recently, Jing et al. investigated the validity of the Westervelt equation through comparison with the more precise nonlinear wave equation that is reduced to the Westervelt equation when the second-order Lagrangian density vanishes [9]. They used the angular spectrum method and found that the Westervelt is quite accurate in theoretically describing nonlinear waves from a spherically curved focused transducers having an aperture angle of 80°. The methods and formulations mentioned above are well developed for predicting nonlinear fields from unfocused or focused intense sources with circular or rectangular apertures. In addition, source excitations in the cw and pulsed modes are considered. A recently published monograph contains details on various current approaches and simulation models [10,11].

In order to adequately formulate the effect of diffraction and provide greater insight into the wide-angle propagation of sound beams, we use an alternative approach, namely, the split-step Padé approximation, which was first proposed by Collins for underwater acoustics [12]. To this end, the present report begins with a brief description of the split-step Padé approximation. Numerical

* Corresponding author. Tel.: +81 42 443 5161; fax: +81 42 443 5210.
E-mail address: kamakura@ee.uec.ac.jp (T. Kamakura).

0041-624X/$ - see front matter © 2012 Elsevier B.V. All rights reserved.
http://dx.doi.org/10.1016/j.ultras.2012.08.008

demonstrations of sound beam profiles in linear fields are then presented. In addition, the theory and numerical scheme are extended to beam profiles in the nonlinear regime, where the Westervelt equation is used as an appropriate model of wave equations with quadratic nonlinearity. All simulations presented herein are limited to beams from ultrasound sources with circular apertures.

As far as we know, there has been no report that describes wide-angle propagation approaches for predicting parametric sound fields formed by intense bi-frequency waves. In order to demonstrate the effectiveness of the proposed approach for parametric sounds, we perform an experiment in air using a powerful ultrasound source with a circular aperture driven by a bi-frequency signal of 36 kHz and 40 kHz and compare the results carefully with the corresponding simulated results.

2. Theoretical background

2.1. Model equation

Let us assume that ultrasound beams radiated from a powerful piston source are propagating in a homogeneous and viscous fluid. The propagation of such intense beams is theoretically described by the following Westervelt equation with quadratic nonlinearity [1]:

$$\nabla^2 p - \frac{1}{c_0^2}\frac{\partial^2 p}{\partial t^2} + \frac{b}{\rho_0 c_0^4}\frac{\partial^3 p}{\partial t^3} = -\frac{\beta}{\rho_0 c_0^4}\frac{\partial^2 p^2}{\partial t^2}, \tag{1}$$

where p is the sound pressure, c_0 is the speed of sound at infinitesimal amplitude, b is the diffusivity related to sound absorption, ρ_0 is the medium density, and β is the coefficient of nonlinearity. Substituting the retarded time $t' = t - z/c_0$ into Eq. (1), the second term of the left-hand side in Eq. (1) disappears, and the following equation is obtained:

$$\frac{\partial^2 p}{\partial t' \partial z} = \frac{c_0}{2}\left(\nabla_\perp^2 + \frac{\partial^2}{\partial z^2}\right)p + \frac{b}{2\rho_0 c_0^3}\frac{\partial^3 p}{\partial t'^3} + \frac{\beta}{2\rho_0 c_0^3}\frac{\partial^2 p^2}{\partial t'^2}, \tag{2}$$

where $\nabla_\perp^2 = \partial^2/\partial x^2 + \partial^2/\partial y^2$ is the two-dimensional Laplacian in the x–y plane perpendicular to the z-axis of beam propagation. For circularly symmetric sound fields, $\nabla_\perp^2 = \partial^2/\partial r^2 + (1/r)\partial/\partial r$ ($r = \sqrt{x^2 + y^2}$). By introducing the dimensionless variables of $\bar{p} = p/p_0$, $\tau = \omega t'$, $\xi = r/a$, $\sigma = z/R_d$, and $\bar{\nabla}_\perp^2 = \partial^2/\partial\xi^2 + (1/\xi)\partial/\partial\xi$, Eq. (2) can be rewritten in dimensionless form as follows:

$$\frac{\partial^2 \bar{p}}{\partial\tau\partial\sigma} = \frac{1}{4}\bar{\nabla}_\perp^2 \bar{p} + \varepsilon\frac{\partial^2 \bar{p}}{\partial\sigma^2} + \alpha R_d \frac{\partial^3 \bar{p}}{\partial\tau^3} + \frac{N}{2}\frac{\partial^2 \bar{p}^2}{\partial\tau^2}, \tag{3}$$

where a is the radius of the circular aperture, p_0 is the pressure amplitude on the source face, ω is the angular frequency of ultrasound, R_d is the Rayleigh distance defined by $ka^2/2$, and k is the wavenumber ω/c_0. In ordinary ultrasound waves, $\varepsilon = 1/(ka)^2$ becomes much smaller than unity because $ka \gg 1$. In Eq. (3), $\alpha = b\omega^2/2\rho_0 c_0^3$ is the absorption coefficient. This formula presupposes that sound absorption obeys the frequency-squared law. Otherwise, appropriate modification is required for the formula, for example, in air and biological media. Moreover, $N = R_d/x_s$ is a dimensionless nonlinearity coefficient, in which $x_s = \rho_0 c_0^3/\beta\omega p_0$ is the shock formation distance for a lossless plane wave.

Eq. (3) includes the combined effects in the fundamental characteristics of sound beams. The first term on the right-hand side accounts for diffraction, and the third term represents sound absorption. The last term on the right-hand side is related to the nonlinearity of the medium. In the absence of diffraction, absorption, and nonlinearity, the remaining two terms are collected to obtain

$$\frac{\partial}{\partial\sigma}\left[\frac{\partial}{\partial\tau} - \varepsilon\frac{\partial}{\partial\sigma}\right]\bar{p} = 0. \tag{4}$$

This equation has the solution $\bar{p} = F_+(\tau) + F_-(\tau + \sigma/\varepsilon) = F_+(\omega t') + F_-(\omega t' + 2kz) = F_+(\omega t - kz) + F_-(\omega t + kz)$, where F_+ and F_- are arbitrary functions. Consequently, Eq. (4) represents plane waves traveling individually in the positive and negative directions.

As a rule, it is difficult to solve Eq. (3) analytically and/or computationally while taking into account all of the terms, even for the case in which the nonlinearity is weak enough to use a quasi-linear approach. Instead, we herein use the operator splitting scheme that is often used to numerically solve nonlinear wave equations.

2.2. Operator splitting

Over sufficiently small traveling steps of a sound wave, the effects of diffraction, absorption, and nonlinearity may be assumed to be independent of each other. We can then divide Eq. (3) into the following three equations:

$$\frac{\partial^2 \bar{p}}{\partial\tau\partial\sigma} = \frac{1}{4}\bar{\nabla}_\perp^2 \bar{p} + \varepsilon\frac{\partial^2 \bar{p}}{\partial\sigma^2}, \tag{5}$$

$$\frac{\partial^2 \bar{p}}{\partial\tau\partial\sigma} = \alpha R_d \frac{\partial^3 \bar{p}}{\partial\tau^3}, \tag{6}$$

$$\frac{\partial^2 \bar{p}}{\partial\tau\partial\sigma} = \frac{N}{2}\frac{\partial^2 \bar{p}^2}{\partial\tau^2}. \tag{7}$$

Eqs. (5)–(7) are solved independently by using the output data of one equation as the input data of the next equation over each small step in σ.

2.2.1. Eq. (5): Diffraction stage

Let the sound pressure be $\bar{p} = (qe^{j\tau} - q^* e^{-j\tau})/2j$ by assuming that the beam is in a steady state motion, where the superscript $*$ signifies the complex conjugate of the pressure q. Substitution of $\bar{p}$ into Eq. (5) yields

$$\left(\frac{\partial^2}{\partial\sigma^2} - j\frac{1}{\varepsilon}\frac{\partial}{\partial\sigma} + \frac{1}{4\varepsilon}\bar{\nabla}_\perp^2\right)q = 0. \tag{8}$$

Factoring Eq. (8) and keeping the terms representing outgoing waves in the positive z direction, we obtain

$$\frac{\partial q}{\partial\sigma} = -j\frac{1}{2\varepsilon}\left(\sqrt{1 + \varepsilon\bar{\nabla}_\perp^2} - 1\right)q. \tag{9}$$

The wave operator $\bar{\nabla}_\perp^2$ is equivalent to $-(k_r/k)^2$ in the k-space, where k_r is the wavenumber in the radial direction. For a sound beam to be collimated and its frequency to be high, both k_r/k and $\varepsilon = 1/(ka)^2$ are smaller than unity. Hence, $\varepsilon\bar{\nabla}_\perp^2$ in Eq. (9) is so small that we can approximate the square-root term with the help of a Taylor power series:

$$\sqrt{1 + \varepsilon\bar{\nabla}_\perp^2} = 1 + \frac{\varepsilon}{2}\bar{\nabla}_\perp^2 - \frac{\varepsilon^2}{8}\left(\bar{\nabla}_\perp^2\right)^2 + \cdots. \tag{10}$$

When the first two terms in the right-hand side of Eq. (10) are retained, Eq. (9) is reduced to

$$\frac{\partial q}{\partial\sigma} = -j\frac{1}{4}\bar{\nabla}_\perp^2 q. \tag{11}$$

The model equation obtained in this manner is a standard parabolic equation (PE) that serves as a basis for the derivation of the KZK equation. The PE is actually simple in form and is readily solvable analytically. However, due to such a rough approximation, the region of validity is restricted to a propagation angle of no more than ±20° with respect to the z axis and to a field of several wavelengths away from the sound source [1–3]. As expected, the approximation accuracy is improved for propagation angles of greater than 20° by including higher-order terms in Eq. (10).

However, the higher-order PE methods based on a Taylor series are intrinsically inefficient because several terms are essentially required in order to validate wide-angle propagation [13].

Alternatively, we apply the split-step Padé approximation to Eq. (9). Here, we first obtain the solution of Eq. (9) at $\sigma + \Delta\sigma$. We then apply the Padé approximation [12]:

$$q(\xi,\sigma+\Delta\sigma)=e^{j(1-\sqrt{1+\varepsilon X})\Delta\sigma/2\varepsilon}q(\xi,\sigma)=\left(1+\sum_{i=1}^{N}\frac{a_iX}{1+b_iX}\right)q(\xi,\sigma), \quad (12)$$

where $\Delta\sigma$ is a small grid in the σ coordinate. In Eq. (12), the differential operator $\bar{\nabla}_\perp^2$ is replaced with X for simplicity. In order to reduce the number of differential operators X, we may transform the equation as follows:

$$q(\xi,\sigma+\Delta\sigma)=\left(1+\sum_{i=1}^{N}\frac{a_i}{b_i}-\sum_{i=1}^{N}\frac{a_i}{b_i}\frac{1}{1+b_iX}\right)q(\xi,\sigma), \quad (13)$$

where a_i and $b_i (i = 1,\ldots,N)$ are the Padé coefficients and are numerically determined by equating the first $2N$ derivatives of both the equations of the center and right-hand side in Eq. (12).

The solution of Eq. (13) is obtained in accordance with the following two steps:

- *Step 1:* We obtain the pressures q_i along the radial direction ξ at $\sigma + \Delta\sigma$ by solving reduced equations:

$$(1+b_iX)q_i(\xi,\sigma+\Delta\sigma)=q(\xi,\sigma) \quad (14)$$

  subject to the known pressure data q at σ for $i = 1$ to N. More specifically, the right-hand side of Eq. (14) contains the known values of q along the radial direction with the step of $\Delta\xi$, whereas the left-hand side contains the unknown values of q_i at the next step $\sigma + \Delta\sigma$ along the radial steps. This is a typical implicit method to solve Eq. (14) in a finite difference scheme.
- *Step 2:* Using the solutions q_i, Eq. (13) is represented as

$$q(\xi,\sigma+\Delta\sigma)=\left(1+\sum_{i=1}^{N}\frac{a_i}{b_i}\right)q(\xi,\sigma)-\sum_{i=1}^{N}\frac{a_i}{b_i}q_i(\xi,\sigma+\Delta\sigma).$$

Thus, if the pressure at σ is known in advance, we obtain the unknown pressure q at $\sigma + \Delta\sigma$ in a step-by-step manner. Here, q at the first step is the pressure amplitude at $\sigma = 0$ and is initially specified by appropriate boundary conditions on the source face.

2.2.2. Eq. (6): Absorption stage

Using the complex pressure q, we rewrite Eq. (6) as follows:

$$\frac{dq}{d\sigma}=-\alpha R_d q. \quad (15)$$

This equation is readily integrated with respect to σ, which is expressed as

$$q(\sigma+\Delta\sigma)=e^{-\alpha R_d\Delta\sigma}q(\sigma). \quad (16)$$

As mentioned above, the Westervelt equation assumes that the sound absorption obeys the frequency-squared law. In air and biological media especially, an appropriate modification of α is needed depending on the absorption mechanism.

2.2.3. Eq. (7): Nonlinearity stage

Due to the presence of the nonlinear term $\bar{p}^2$ in Eq. (7), pressure waveforms are distorted during propagation, and several harmonics and/or combination frequency components are inherently generated. Here, we set the nth harmonic pressure component as $\bar{p}_n$ and the corresponding complex pressure as q_n. Then, it follows that

$$\bar{p}_n=\frac{1}{2j}\left(q_ne^{jn\tau}-q_n^*e^{-jn\tau}\right). \quad (17)$$

Substitution of Eq. (17) into Eq. (7) yields the equation of the n-th harmonic:

$$\frac{dq_n}{d\sigma}=\frac{nN}{4}\left(\sum_{l=1}^{n-1}q_lq_{n-l}-2\sum_{l=n+1}^{M}q_lq_{l-n}^*\right), \quad (18)$$

where M is the number of harmonics retained in computation. This number is usually determined by the value of N. The larger the value of N, the greater the number of harmonics that must be retained. Naturally, sound absorption, numerical accuracy, and computer power are additional factors for the determination of M.

The most efficient and straightforward method for solving Eq. (18) is to use the explicit Euler method. Over small steps of $\Delta\sigma$, the pressure component q_n at $\sigma + \Delta\sigma$ is approximately provided by various harmonic components at σ:

$$q_n(\xi,\sigma+\Delta\sigma)=q_n(\xi,\sigma)+\frac{nN\Delta\sigma}{4}\left(\sum_{l=1}^{n-1}q_l(\xi,\sigma)q_{n-l}(\xi,\sigma)-2\sum_{l=n+1}^{M}q_l(\xi,\sigma)q_{l-n}^*(\xi,\sigma)\right). \quad (19)$$

3. Numerical examples

3.1. Linear field

In order to demonstrate the effectiveness of the Padé approximation, we present a few typical numerical examples for sound beam behavior in a lossless linear field. Suppose that an ultrasound piston source with a circular aperture of radius $a = 5$ cm radiates a 40-kHz sinusoidal wave in air ($c_0 = 340$ m/s). In addition, the distribution of pressure amplitude over the source face is assumed to be uniform:

$$\bar{p}(\xi,\sigma)|_{\sigma=0}=\begin{cases}1 & (0\leqslant\xi\leqslant 1)\\ 0 & (\xi>1).\end{cases} \quad (20)$$

The pressure q at $\sigma + \Delta\sigma$ can be obtained numerically from the data at σ through the process of Steps 1 and 2. An even grid-spacing system is introduced in the integration region: $0 \leqslant \xi \leqslant \xi_{max}$ and $0 \leqslant \sigma < \infty$. Concretely, the values of grid sizes in both directions are assigned to be $\Delta\xi = 0.025$ and $\Delta\sigma = 2 \times 10^{-4}$ based on empirical data [14]. There are 1200 grid-points in the ξ coordinate, so that $\xi_{max} = 30$. This corresponds to $0 \leqslant r \leqslant 1.5$ m in the actual radial dimension. Furthermore, for simplicity, only two terms remain in the Padé approximation ($N = 2$).

Fig. 1 shows the beam patterns at $z = 2$ m, where the abscissa indicates the radial distance r from the z-axis, and the ordinate indicates the relative pressure amplitude $\bar{p} = p/p_0$. The solid line in the figure denotes the pattern using the split-step Padé approximation method proposed herein. The dotted line denotes the pattern based on the PE of Eq. (11), which is solved analytically:

$$q=j\frac{2}{\sigma}e^{-j\frac{\xi^2}{\sigma}}\int_0^1 J_0\left(\frac{2\xi}{\sigma}\xi'\right)e^{-j\frac{\xi'^2}{\sigma}}\xi'd\xi', \quad (21)$$

where $J_0(\cdot)$ is the zero-th order Bessel function. For comparison, the pattern obtained using the Rayleigh integral solution is indicated by the dashed line. Based on the source conditions, the Rayleigh distance R_d is 92 cm. The receiving point at $z = 2$ m is then approximately twice as far from the source, as compared to the Rayleigh distance, and is located almost in the far field. The resultant separation in the main-lobe and side-lobes is clearly observed.

Incidentally, the Rayleigh integral solution associated with the boundary condition of uniform particle-velocity u_0 on the source

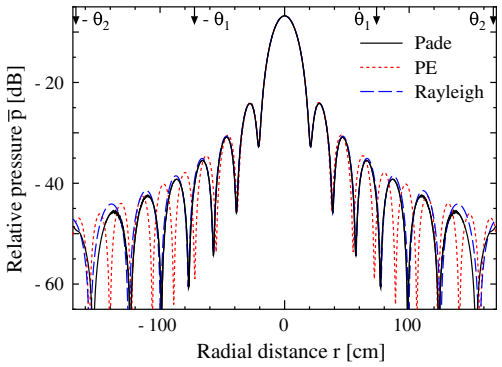

Fig. 1. Beam patterns of a 40-kHz airborne ultrasound wave at $z = 2$ m from a piston source having an aperture of 5 cm in radius ($ka = 37$). Split-step two-term Padé approximation (solid line), standard PE solution (dotted line), and analytically exact solution obtained using the Rayleigh integral (dashed line). θ_1 and θ_2 indicate propagation angles of 20° and 40°, respectively.

face provides the exact solution for a piston source in an infinite rigid baffle:

$$q = j\frac{\omega\rho_0}{2\pi}\int\int_{S_0}\frac{u_0}{p_0}\frac{e^{-jk(R-z)}}{R}dS, \tag{22}$$

where R is the distance between the coordinates of a point source on the aperture S_0 and those of the receiver, and dS is the area element used for integration. If the relation of plane wave impedance $u_0 = p_0/\rho_0 c_0$ holds on the aperture, Eq. (22) is reduced to the following equation with uniform pressure distribution over the source face:

$$q = j\frac{k}{2\pi}\int\int_{S_0}\frac{e^{-jk(R-z)}}{R}dS. \tag{23}$$

The dashed beam pattern in Fig. 1 is obtained using Eq. (23). Likewise, the split-step Padé and PE approximations both specify uniform pressure over the source face. It is therefore appropriate to compare the field characteristics of the three curves because their boundary conditions are the same at least over the aperture. Obviously, the Padé solution agrees well with the Rayleigh integral within a radial distance of $r = \pm 1.4$ m, which corresponds to an angle range of approximately ±40° and is twice as wide as the propagation angle of the PE solution.

Importantly, the side-lobes predicted by the PE solution, especially those far from the z-axis, tend to more closely approach the z-axis, i.e., the spreading of the beam is slightly suppressed. A similar tendency is observed elsewhere. (For example, see Fig. 5 in Ref. [6]) In fact, the operator $\sqrt{1+\varepsilon\bar{\nabla}_\perp^2}$ in the left-hand side of Eq. (10) is equivalent to k_z/k in the k-space, where k_z is the wavenumber in the axial direction and is associated with k_r by $k_z = \sqrt{k^2 - k_r^2}$. Thus, based on Eq. (10), the PE operator $1 + (\varepsilon/2)\bar{\nabla}_\perp^2$ is always larger than the wave operator $\sqrt{1+\varepsilon\bar{\nabla}_\perp^2}$ because the difference of the operators becomes roughly $-(\varepsilon^2/8)(\bar{\nabla}_\perp^2)^2$ and takes negative values $-(\varepsilon^2/8)\{-(k_r a)^2\}^2 = -(1/8)(k_r/k)^4$ in the k-space. Hence, plane wave modes in the PE approach are actually overestimated, so that beam spreading should be suppressed as a whole.

3.2. Extension to nonlinear field analysis

Next, we turn to the solution of the Westervelt equation based on the operator splitting method. Let the complex pressure of the nth harmonic be q_n. The pressure must then satisfy the wave equation given by Eq. (5):

$$\left(\frac{\partial^2}{\partial\sigma^2} - j\frac{n}{\varepsilon}\frac{\partial}{\partial\sigma} + \frac{1}{4\varepsilon}\bar{\nabla}_\perp^2\right)q_n = 0. \tag{24}$$

This equation is the same as Eq. (8) if the coefficient n/ε is replaced with $1/\varepsilon$. We can then obtain the solution of Eq. (24) by simply modifying Eq. (12) under such a simple transformation. In addition, for higher harmonics, it is expected that the second term of Eq. (24) will become larger than the first term. In other words, the effects of the second derivative with respect to σ on sound pressure magnitudes become weaker for higher harmonics.

The form for sound absorption is basically the same as that of Eq. (16):

$$q_n(\sigma + \Delta\sigma) = e^{-\alpha_n R_d \Delta\sigma} q_n(\sigma), \tag{25}$$

where α_n is the absorption coefficient at frequency $n\omega$. The explicit solution of the nonlinear equation given by Eq. (7) is already given by Eq. (19).

Over sufficiently small steps, the effects of diffraction, absorption, and nonlinearity may be assumed to be independent of each other. Therefore, we use the concept of a first-order operator-splitting scheme. The three calculation steps represented by Eqs. (5)–(7) are implemented sequentially every $\Delta\sigma$ up to the position of a receiver.

Let us compare the simulation results obtained using the split-step Padé-based model equation and those obtained using the KZK equation. The KZK equation is derived by removing the second term of the right-hand side on Eq. (3), i.e.,

$$\frac{\partial^2\bar{p}}{\partial\tau\partial\sigma} = \frac{1}{4}\bar{\nabla}_\perp^2\bar{p} + \alpha R_d\frac{\partial^3\bar{p}}{\partial\tau^3} + \frac{N}{2}\frac{\partial^2\bar{p}^2}{\partial\tau^2}. \tag{26}$$

Fig. 2 shows the propagation curves along the beam axis and the beam patterns at $z = 2$ m of the first three harmonics for a 40-kHz initial wave with a pressure amplitude of 125 dB ($p_0 = 50$ Pa). The radius of the present piston source is 7.5 cm. Then, $ka = 55$. Since $R_d = 2.08$ m and $x_s = 3.13$ m, the dimensionless nonlinearity

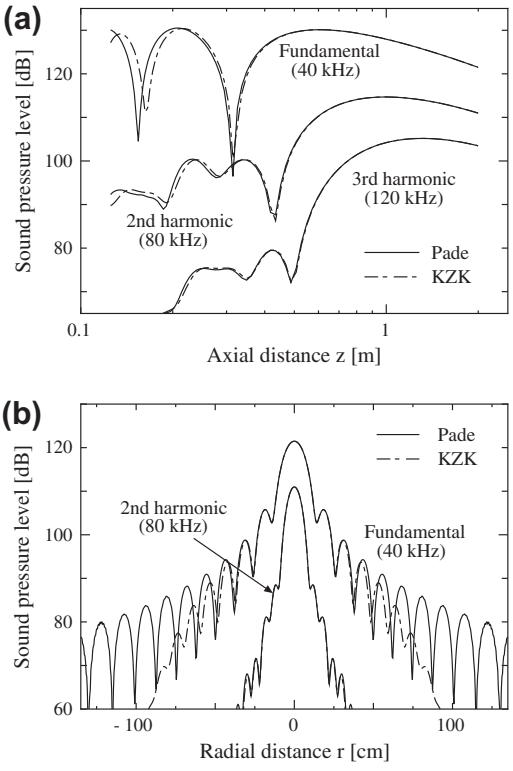

Fig. 2. On-axis pressure curves (a) and beam patterns (b) at $z = 2$ m for the first two or three harmonics. An ultrasound source with a circular aperture of 7.5 cm radiates a 40-kHz sinusoidal wave. The source pressure level is 125 dB.

coefficient becomes $N = 0.66$. This magnitude implies that the nonlinearity is moderate, so that the first 10 harmonics are retained in the calculation ($M = 10$). Since atmospheric temperature and relative humidity affect sound absorption in air, we set the atmospheric temperature to be 20 °C and the relative humidity to be 50%. The grid sizes for the Padé method and the KZK equation are the same and are slightly different from the numerical parameters in Fig. 1: $\Delta\xi = 0.02$, $\Delta\sigma = 2 \times 10^{-4}$, and $\xi_{max} = 24$.

The solid lines in the figure denote the pressure curves obtained by the proposed method involving the Padé method, and the dot-dashed lines denote the pressure curves obtained using the KZK model equation. As shown in Fig. 2a, there are somewhat noticeable differences between the two approaches in the near field less than 20 cm from the source. However, the differences become smaller for higher harmonics [13].

Relatively striking differences appear in both the beam patterns of the 40-kHz fundamental components in Fig. 2b as the receiver moves away from the beam axis. More precisely, the pressure amplitudes predicted by the KZK equation are underestimated in the region in which r is greater than 50 cm ($\theta \simeq 15°$). Again, note that the third or more outer side-lobes tend to approach the z-axis, possibly due to the reason described by Fig. 1.

Fig. 3 shows a quantitative comparison between the experiment and theory when a bi-frequency ultrasound wave is radiated from a powerful source. Since the primary frequencies are 36 kHz and 40 kHz, the difference frequency or parametric frequency is 4 kHz. An experiment was performed using an ultrasonic emitter that consists of 207 small piezoelectric ceramic transducers of 1 cm in diameter. The aperture of the emitter is approximately circular, having a radius of $a = 7.8$ cm. Keeping $z = 2$ m, a quarter-inch condenser microphone was manually moved in the radial direction by approximately 5-cm steps in order to pick up various frequency components. The on-source pressure amplitudes of the two primary waves were determined by the best fit of curves with measured propagation data along the beam axis for the fundamental pressure by assuming that the pressure distribution over the source face is uniform. The resultant amplitudes were estimated to be 44.8 Pa (SPL = 124 dB) and 71 Pa (SPL = 128 dB) for the 36-kHz and 40-kHz waves, respectively. The room temperature (21 °C) and relative humidity (64%) were almost unchanged during the experiment. Moreover, the noise floor in the experimental set-up has a sound pressure level of approximately 25 dB.

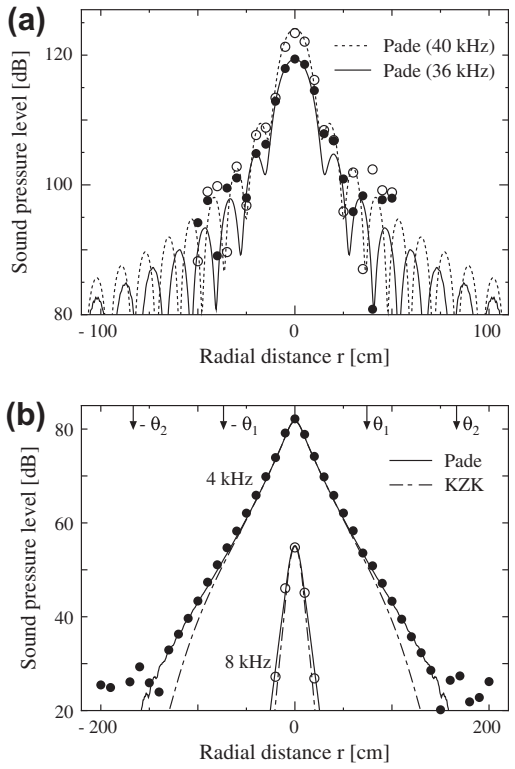

Fig. 3. Beam patterns of the primary waves (a) and the secondary waves at $z = 2$ m. An ultrasonic emitter with a circular aperture of 7.8 cm in radius radiates 36-kHz and 40-kHz primary sound beams. The source pressure levels p_0 for both the two primary waves are expected to be 124 dB and 128 dB. All of the circles in the figures denote experimental data. θ_1 and θ_2 indicate propagation angles of 20° and 40°, respectively.

The measured beam patterns of the primary waves are practically in good agreement with the present split-step Padé scheme within the measured range of $r \simeq 30$ cm, especially within the main-lobe and at least the first two side-lobes. However, somewhat poor agreement is observed in the third or more outer side-lobes, probably due to the non-uniformity in the source pressure (see Appendix A). Such discrepancies appear not to generate serious errors in predicting parametric sounds, because parametric sounds are created by the spatial distribution of the virtual sources that originate from the mutual interaction of the primary waves. Moreover, the primary sound pressures in the side lobes, which are 20 dB lower than those in their main lobes, for example, contribute to only 1% of the creation of parametric sounds. In fact, Fig. 3b reveals that the 4-kHz parametric sound beam agrees excellently with the theoretical predictions up to the radial range of $r = \pm 1.5$ m, which corresponds to a beam propagation angle, θ, of approximately ±40 °. For comparison, the beam pattern curves predicted by the KZK equation are indicated by dot-dashed lines. Needless to say, the applicability of the KZK equation is limited to narrow beams that are roughly half the angle predicted by the Padé approach. Similarly, the measured 8-kHz beam pattern agrees well with numerical simulations. Unfortunately, the beam is so narrow that we cannot determine which of the curves of the two theories is in better agreement with the measured data. More precise measurements are needed in order to make this determination.

Incidentally, the runtime in computation is significantly dependent on various factors, such as the CPU, the programming code, and the grid sizes. In order to complete the simulations in Fig. 3, it took 2′35″ for the Padé approach and 6′10″ for the KZK equation when implementing on a PC with Intel(R) Core2 Quad CPU (Q9550) and using the Intel Visual Fortran compiler. It is anticipated that considerable runtime savings would be achievable using the second-order operator-splitting for field simulation [6].

4. Conclusions

In order to solve the Westervelt nonlinear model equation for the problem of wide-angle beam propagation, we have introduced the split-step Padé approximation, which is an efficient numerical simulation of various theoretical approaches. Despite the use of only the two Padé terms, the applicability limit of the propagation angle has been extended to approximately ±40° and to an angle twice as wide as that of the KZK equation. We have carried out an experiment using a bi-frequency airborne ultrasound in order to demonstrate the effectiveness of the application of the split-step Padé approach to nonlinear field analysis. It has been confirmed that the present model and numerical techniques are in extremely close agreement with the measured data for parametric sounds, even when the approach of the KZK equation fails.

Acknowledgments

We greatly appreciate the helpful discussions of Tsuneo Ishiwata and wish to thank Gaku Kubota for his assistance in conducting the experiment. The present study was supported in part by a

Grant-in-Aid for Scientific Research(B) No. 22360094 from the Japan Society for the Promotion of Science and by the Regional Innovation Strategy Support Program 2011 from the Ministry of Education, Culture, Sports, Science and Technology.

Appendix A. Random allocation of transducers

Generally, the electro-acoustic conversion efficiency of a piezoelectric ceramic transducer varies from unit to unit. As an example, Fig. A1 shows the amplitudes and phases of sound pressures obtained from 456 transducers that are structurally similar to the transducers we used for the present experiment [15]. We really notice that the variance of the conversion efficiency is relatively large: the standard deviation of the pressure amplitude is $\sigma' = 4.54$ Pa and attains 16% of the average value $p_0 = 27.6$ Pa.

Let us assume that sound waves radiated from the transducer are propagating in free space. In this case, the complex sound pressure p' is generally given by the Rayleigh integral formula of Eq. (23):

$$p' = p_0 q e^{jkz} = j\frac{kp_0}{2\pi}\int\int_{S_0}\frac{e^{-jkR}}{R}dS, \tag{A1}$$

where S_0 is the aperture area. The face of the ultrasonic emitter that is composed of many transducers is not planar but uneven owing to the circular horns of the transducers. Since it is difficult to strictly simulate the field by taking account of such involved boundary conditions, we approximate the above Rayleigh integral as:

$$p' \simeq j\frac{k}{2\pi}\sum_{n=1}^{N}p_0(n)\frac{e^{-jkR_n}}{R_n}\Delta S = j\frac{kS_0}{2\pi N}\sum_{n=1}^{N}p_0(n)\frac{e^{-jkR_n}}{R_n}, \tag{A2}$$

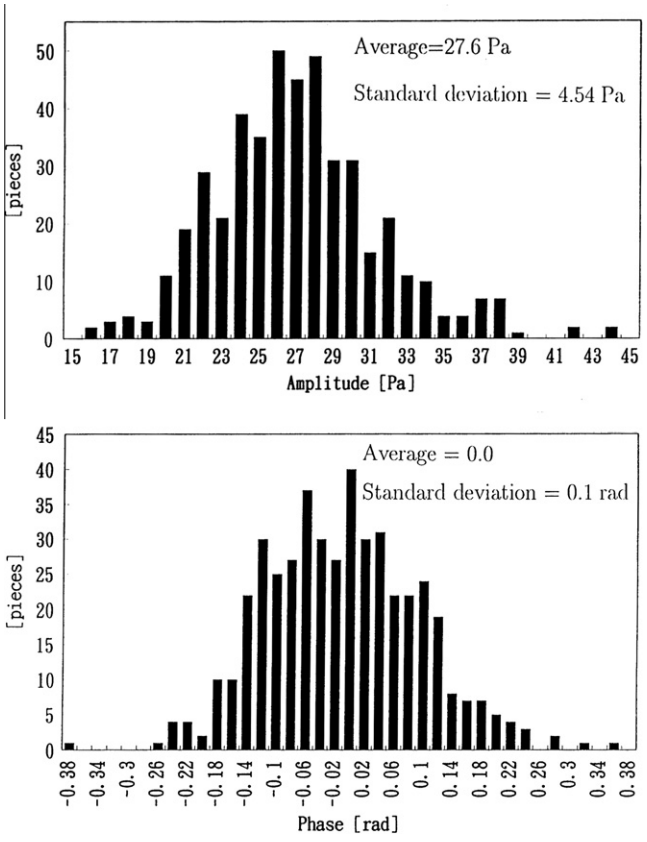

Fig. A1. Variations of the received pressure amplitudes and phases obtained from 456 small piezoelectric ceramic transducers [15]. The input voltage applied to each transducer is $6V_{p-p}$ and the driving frequency is 30 kHz. The separation distance between the transducer and a quarter-inch condenser microphone is 1 cm.

by assuming that all the transducers are omnidirectional and each transducer has the individual sensitivity. Besides, we ignore the mutual impedance of the transducer array that may affect the formation of sound fields for simplicity. In Eq. (A2), N is the number of transducers, R_n is the distance between the coordinates of a cone's center and those of the receiver, and the transducer area is approximately given by $\Delta S = S_0/N$.

Hypothetically, consider the situation where the present ultrasonic emitter is one of many possible sample emitters that are composed through random allocation of ultrasonic transducers with statistical characteristics shown in Fig. A1. We do not herein take account of the phase variation of the individual transducer for simplicity. From Eq. (A2), the ensemble average of the received pressure p' is given by

$$\langle p'\rangle = j\frac{kS_0}{2\pi N}\sum_{n=1}^{N}\langle p_0(n)\rangle\frac{e^{-jkR_n}}{R_n}, \tag{A3}$$

where the symbol $\langle\ \rangle$ indicates ensemble averaging and $p_0(n)$ is a random variable that determines the pressure amplitude on the source. Since $\langle p_0(n)\rangle$ is equal to the mean value p_0, Eq. (A3) becomes

$$\langle p'\rangle = j\frac{kS_0p_0}{2\pi N}\sum_{n=1}^{N}\frac{e^{-jkR_n}}{R_n}. \tag{A4}$$

Basically, this equation is the same as Eq. (A2) when the pressure amplitude is distributed uniformly over the source.

Next, we consider the variance of the pressure that is defined as the mean square value of p' about its mean value $\langle p'\rangle$.

$$\langle (p'-\langle p'\rangle)(p'-\langle p'\rangle)^*\rangle = \left(\frac{kS_0}{2\pi N}\right)^2\sum_{n=1}^{N}\sum_{m=1}^{N}\langle (p_0(n)-p_0)(p_0(m)-p_0)\rangle \times\frac{e^{-jk(R_n-R_m)}}{R_nR_m}. \tag{A5}$$

The random variables $p_0(n)$ and $p_0(m)$ are assumed to be uncorrelated, then

$$\langle (p_0(n)-p_0)(p_0(m)-p_0)\rangle = \sigma'^2\delta(n-m), \tag{A6}$$

where σ'^2 is the variance defined as $\sigma'^2 = \langle (p_0(n)-p_0)^2\rangle$ and $\delta(n)$ is the unit impulse function. From Eqs. (A-5) and (A-6), the variance of the pressure amplitude yields

$$\langle (p'-\langle p'\rangle)(p'-\langle p'\rangle)^* > = \left(\frac{kS_0}{2\pi N}\right)^2\sum_{n=1}^{N}\sum_{m=1}^{N}\sigma'^2\delta(n-m)\frac{e^{-jk(R_n-R_m)}}{R_nR_m} = \left(\frac{kS_0}{2\pi N}\right)^2\sigma'^2\sum_{n=1}^{N}\frac{1}{R_n^2}. \tag{A7}$$

Interestingly, the pressure variance is independent of the emitter directivity. When the receiver is located on the z-axis in the far-field, the mean pressure amplitude expressed by Eq. (A4) gives approximately

$$p_m = |p'|_{z\to\infty} \simeq \frac{kS_0p_0}{2\pi N}N\frac{1}{z} = \frac{kS_0p_0}{2\pi z}, \tag{A8}$$

because of $R_n \sim z$. Similarly, the standard deviation of the pressure is the square root of Eq. (A7), being given by

$$p_s = \sqrt{\langle (p'-\langle p'\rangle)(p'-\langle p'\rangle)^* >}_{z\to\infty} \simeq \frac{kS_0\sigma'}{2\pi z\sqrt{N}}. \tag{A9}$$

The coefficient of variance that is defined as p_s/p_m is $\sigma'/\sqrt{N}p_0$. It is therefore expected that the pressure amplitude radiated from an ultrasonic emitter with a randomly distributed pressure amplitude with the mean value p_0 and standard deviation σ' has a possibility of randomness in amplitude with the deviation about the pressure mean, but its magnitude is inversely proportional to $\sqrt{N}$. Especially, the effect of randomness in transducer's sensibility on

received pressure amplitudes should be mainly observed in the sidelobes and dips of the beam pattern because the variance is independent of the emitter directivity.

References

[1] M.F. Hamilton, C.L. Morfey, Model equations, in: M.F. Hamilton, D.T. Blackstock (Eds.), Nonlinear Acoustics, Academic Press, San Diego, 1998 (Chapter 3).
[2] J.H. Ginsberg, M.F. Hamilton, Computational methods, in: M.F. Hamilton, D.T. Blackstock (Eds.), Nonlinear Acoustics, Academic Press, San Diego, 1998 (Chapter 11).
[3] F.B. Jensen, W.A. Kuperman, M.B. Porter, H. Schmidt, Computational Ocean Acoustics, AIP, New York, 2000 (Chapter 6).
[4] P.T. Christopher, K.J. Parker, New approaches to nonlinear diffractive field propagation, J. Acoust. Soc. Am. 90 (1991) 488–499.
[5] J. Tavakkoli, D. Cathignol, R. Souchon, O.A. Sapozhnikov, Modeling of pulsed finite-amplitude focused sound beams, J. Acoust. Soc. Am. 104 (1998) 488–499.
[6] R.J. Zemp, J. Tavakkoli, R.S.C. Cobbold, Modeling of nonlinear ultrasound propagation in tissue from array transducers, J. Acoust. Soc. Am. 113 (2003) 139–152.
[7] J. Huijssen, A. Bouakaz, M.D. Verweij, J.N. de Jong, Simulations of the nonlinear acoustic pressure field without using the parabolic approximation, 2003, in: IEEE Ultrasonics Symposium, 2003, pp. 1851–1854.
[8] J. Huijssen, M.D. Verweij, An iterative method for the computation of nonlinear, wide-angle, pulsed acoustic fields of medical diagnostic transducers, J. Acoust. Soc. Am. 127 (2010) 33–44.
[9] Y. Jing, D. Shen, G.T. Clement, Verification of the Westervelt equation for focused transducers, IEEE Trans. UFFC 58 (2011) 1097–1101.
[10] M.D. Verweij, J. Huijssen, Computational methods for nonlinear acoustic wavefields in homogeneous media, in: C. Vanhille, C. Campos-Pozuelo (Eds.), Computational Methods in Nonlinear Acoustics: Current Trends, Research Signpost, Kerala, 2011 (Chapter 1).
[11] F. Coulouvrat, R. Marchiano, M. Rénier, One-way approaches for the simulation of acoustical shock waves propagation in heterogeneous media – application to sonic boom, in: C. Vanhille, C. Campos-Pozuelo (Eds.), Computational Methods in Nonlinear Acoustics: Current Trends, Research Signpost, Kerala, 2011 (Chapter 7).
[12] M. Collins, A split-step Padé solution for the parabolic equation method, J. Acoust. Soc. Am. 93 (1993) 1736–1742.
[13] T. Kamakura, M. Akiyama, K. Aoki, A higher-order parabolic equation for describing nonlinear propagation of ultrasound beams, Acoust. Sci. Technol. 25 (2004) 163–165.
[14] I. Aanonsen, Numerical Computation of the Nearfield of a Finite Amplitude Sound Beam, Rep. No. 73, Department of Mathematics, University of Bergen, Bergen, Norway, 1983.
[15] H. Kawashima, K. Aoki, T. Kamakura, Effect of a Variation in Source Pressure Distribution on Nonlinear Sound Field, Technical Report of IEICE US 98-97, 1999 (in Japanese).